MECSOL 2019 - Proceedings of the 7th International Symposium on Solid Mechanics
V. Tita, A. Ferreira, M.L. Ribeiro, A. Vieira and A.T. Beck (Editors), ABCM, Sao Carlos, SP, Brazil, April 15th to 17th, 2019

Assessment of two different constitutive models in High Speed Forming

Andrey Brezolin[1], Tiago dos Santos[2], Pedro A. R. C. Rosa[3], Evandro Paese[4], Martin Geier[5] and Rodrigo Rossi[1]

[1] Departamento de Engenharia Mecânica, Universidade Federal do Rio Grande do Sul, Rua Sarmento Leite, 425, Porto Alegre, RS, 90046-902, Brazil.
[2] Departamento de Engenharia Mecânica, Universidade Federal de Santa Maria, Av. Roraima, 1000, Prédio 7, Santa Maria, RS, 97105-900, Brazil.
[3] Instituto de Engenharia Mecânica, Instituto Superior Tecnico, Universidade de Lisboa, Lisboa, Portugal.
[4] Departamento de Engenharia Mecânica, Universidade de Caxias Sul, Campus Universitário da Região dos Vinhedos, Rua Alameda João Dal Sasso, 800, Bento Gonçalves, RS, 95700-000, Brazil.
[5] Engenharia Mecânica, Escola Politécnica, Universidade do Vale do Rio dos Sinos, Av. Unisinos, 950, São Leopoldo, RS, 93.022-750, Brazil.

Abstract. This work presents a numerical study on strain-rate hardening effects in high-speed forming processes considering isothermal conditions. The whole analysis investigates the influence of the adopted constitutive model on the overall mechanical response. According to results available in the literature, at high strain-rates, as in high-speed forming, pronounced rate-induced hardening is expected to occur. In an effort to capture such phenomenon, the model proposed in (dos Santos et al., 2016; dos Santos, 2016) is adopted. In order to evidence the influence of the adopted constitutive model, two viscoplastic formulations are compared in high-speed forming simulations. That is, numerical results obtained considering dos Santos model are compared to simulations using the traditional Johnson-Cook proposal. Specifically, model parameters adjusted for AA1050 aluminum samples are used. Even though both models were calibrated considering the same material data, substantial contrasts are evidenced in the predicted behavior. The main difference is not only in terms of final displacements but also in terms of the stabilized stress and accumulated viscoplastic strain.

Keywords: Elastoviscoplasticity, Strain-rate hardening, High-speed forming, FEM.

INTRODUCTION

Forming processes involving high velocities of deformation, typically exceeding 100 m/s, also known as high-speed forming processes, have gained the attention of industries around the world in the last decades. By using these processes, engineers have developed a series of new products overcoming some technical issues intrinsically related to the traditional forming process. Among the high-speed processes, one can cite the explosive forming, electro-hydraulic forming and the Electromagnetic forming (EMF). The latter seems quite tempting since it is a process that is mostly clean, has no physical contact between a medium (puncher) and the part to be shaped (workpiece), it is more easily controllable and presents repeatability. Given the fact that this process is devised to produce lightweight parts having a great interest in the automotive and aeronautic industry.

The comprehensive and rational understanding of high-speed forming process, such as the EMF process, is a very complex task since it involves highly nonlinear transient coupled phenomena in electric, magnetic and mechanical fields having also, in some occasions, to introduce heat transfer and contact/impact issues. Focusing on the mechanical behavior one of the main problems is to predict rate effects on the mechanical response. Regarding this matter, several constitutive models have been proposed in the literature. Some of them account only for instantaneous rate effects, maintaining the evolution of the hardening (isotropic) only in terms of the accumulated (visco)plastic strain, see Perzyna (1966, 1971); Perić (1993). While others are formulated based on empirical evidence, such as the Johnson-Cook model, Johnson & Cook (1983). Also, there is the so-called physically-based model as the Mechanical Threshold Stress (MTS) model by Follansbee & Kocks (1988).

In this study, it is proposed the numerical investigation of a particular strain-rate hardening model proposed by dos Santos et al. (2016). This model has the ability to consider the strain-rate hardening using a single internal variable model. See Molinari & Ravichandran (2005) for another example of strain-rate hardening model. Comparisons between the numerical results predicted using dos Santos et al. (2016) model and those predicted by Johnson & Cook (1983) are discussed considering two EMF applications: inward tube forming and free bulging of thin metallic sheets. Both models are calibrated using specific experimental data for commercially pure aluminum (AA1050) (dos Santos, 2016).

VISCOPLASTIC CONSTITUTIVE MODELS

Strain hardening viscoplastic model

In this section, we briefly present the well-known empirical isothermal Johnson-Cook model. As originally presented in Johnson & Cook (1983) this model incorporates the combined effects of strain, strain-rate and temperature. The Johnson-Cook constitutive model is widely employed in technological and scientific modeling and it is available in several commercial FEM packages such as in ABAQUS/Explicit.

The Johnson-Cook model is a viscoplastic model that can be written, for isothermal conditions, as:

$$\sigma = \left(k_A + k_B \bar{\varepsilon}^{k_n}\right)\left[1 + k_C \ln\left(\frac{\dot{\varepsilon}}{\dot{\varepsilon}_0}\right)\right] \tag{1}$$

where σ is the flow stress, $\bar{\varepsilon}$ is the equivalent plastic strain, $\dot{\varepsilon}$ is the plastic strain rate, $\dot{\varepsilon}_0$ is the plastic strain rate at a reference, k_A is the yield stress, k_B and k_n represent the effect of strain hardening, and k_C is a material parameter associated to the strain rate. The experimental data for annealed aluminum AA1050 presented in the work of dos Santos (2016), which employed in the stress evolution the contribution from the yield stress and the viscous stress, served as a basis for the fitting procedures, resulting in the values presented in Table 1. The mass density considered was of 2700 kg/m^3 and the elastic isotropic material parameters of 70 GPa for the Young modulus and 0.33 for the Poisson coefficient were used.

Table 1 – Fitted isothermal Johnson–Cook parameters in accordance to (dos Santos, 2016).

k_A (MPa)	k_B (MPa)	k_C (-)	k_n (-)	ε_0 (-)
41.965	125.323	18.355×10^{-3}	0.6258	0.01

Strain-rate hardening model

In this section we present the viscoplastic model developed in (dos Santos et al., 2016; dos Santos, 2016). This model follows a semi-physical approach and is able to predict the main constitutive features associated with high strain mechanical behavior: strain-hardening, strain-rate hardening and instantaneous rate-sensitivity.

The present viscoplastic formulation uses the von Mises yield criterion with an isotropic hardening, by the following expression:

$$f(\tau, A) = ||\tau^D|| - \sqrt{\frac{2}{3}}(\sigma_y + A)\ , \tag{2}$$

given in terms of Kirchhoff stress τ and the isotropic hardening $A = A_1 + A_2$. Moreover, σ_y is the first yield stress, $||\tau^D|| = \sqrt{\tau^D_{ij}\tau^D_{ij}}$ and τ^D_{ij} is the deviatoric part of τ.

The inelastic evolution is obtained by the following equations:

$$\dot{\varepsilon}^{vp} = \dot{\lambda}\frac{\partial f}{\partial \tau}\ ,\ \dot{A}_1 = \delta(\overline{A}_\infty - A_1)\dot{\varepsilon} \text{ and } A_2 = c\overline{A}_\infty\bar{\varepsilon}\ , \tag{3}$$

where $\dot{\varepsilon}^{vp}$ is the viscoplastic strain rate, $\dot{\lambda}$ is a viscoplastic multiplier and $\overline{A}_\infty$, δ and c are models parameters. The variable $\bar{\varepsilon}$ is the accumulated viscoplastic strain and its rates is defined by the following expression:

$$\dot{\bar{\varepsilon}} := \sqrt{\frac{2}{3}}||\dot{\varepsilon}^{vp}|| = \sqrt{\frac{2}{3}}\dot{\lambda}\ . \tag{4}$$

For a constant strain-rate the hardening variable A from Eq. $(3)_{2,3}$, is calculated by the equation:

$$A = \overline{A}_\infty\left[1 + c\bar{\varepsilon} - \exp(-\delta\bar{\varepsilon})\right]\ , \tag{5}$$

where the saturation of $\overline{A}_\infty$, has to be influenced by previous strain-rate history is expressed as:

$$\overline{A}_\infty := \frac{1}{\bar{\varepsilon}}\int_0^{\bar{\varepsilon}} A_\infty(\dot{\varepsilon})d\varepsilon\ . \tag{6}$$

The parameters δ and A_∞ are obtained by the expressions below:

$$\delta = \left[1-\beta_1(\dot{\bar{\varepsilon}})\right]\delta^{lwr} + \beta_1(\dot{\bar{\varepsilon}})\delta^{up} \,, \tag{7}$$

and

$$A_\infty = \left[1-\beta_2(\dot{\bar{\varepsilon}})\right]A_\infty^{lwr} + \beta_2(\dot{\bar{\varepsilon}})A_\infty^{up} \,, \tag{8}$$

with

$$\beta_i(\dot{\bar{\varepsilon}}) = \left(\frac{\langle \dot{\bar{\varepsilon}} - \dot{\bar{\varepsilon}}_{lwr}\rangle}{\dot{\bar{\varepsilon}}_{up} - \dot{\bar{\varepsilon}}_{lwr}}\right)^{\xi_i} \text{ and } i = \{1,2\} \,, \tag{9}$$

where A_∞^{lwr} and δ_∞^{lwr} are the respective values of A_∞ and δ measured at a lower reference rate $\dot{\bar{\varepsilon}}_{lwr} \ll 1$, and A_∞^{up} and δ_∞^{up} is the value associated with upper reference strain rate $\dot{\bar{\varepsilon}}_{up} \gg 1$. The parameters ξ_1 and ξ_2 are models constants. In the above expression the operator $\langle x\rangle \equiv \frac{1}{2}(x+|x|)$ denotes the Macaulay bracket.

In the present development, a viscoplastic constitutive function $\Theta(\langle f\rangle, A)$ is adopted in a manner that the viscoplastic multiplier λ, is assumed to relate to f and A according to (Perzyna, 1966, 1971):

$$\dot{\lambda} = \Theta(\langle f\rangle, A) \quad , \tag{10}$$

where $\Theta \geq 0$ is the overstress function. For $f \geq 0$, Eq. (10) can be rewritten in the following form:

$$f = \Theta^{-1}(\dot{\lambda}, A) \,. \tag{11}$$

In this work, the following specific form is adopted for the function Θ^{-1} (dos Santos, 2016):

$$f = R(A)\left[(1+\vartheta_1\dot{\lambda})^{1/m} + \vartheta_2\dot{\lambda} - 1\right] \text{ with } R(A) = \sqrt{\frac{2}{3}}(\sigma_y + A) \,, \tag{12}$$

where $1/m$ is a rate sensitivity parameter, ϑ_1 and ϑ_2 are viscosity parameters and $R(A)$ is the radius of the yield locus.

The present constitutive model uses the same elastic properties than the previous model, with addition of the following materials parameters:

Table 2 – Parameters for annealed aluminum AA1050, with $\dot{\varepsilon}_{lwr} = 10^{-4}s^{-1}$ and $\dot{\varepsilon}_{up} = 1.5\times10^{4}s^{-1}$. Source: (dos Santos, 2016)

σ_y	c	δ^{lwr}	δ^{up}	ξ_1	A_∞^{lwr}	A_∞^{up}	ξ_2	ϑ_1	ϑ_2	m
(MPa)	(-)	(-)	(-)	(-)	(MPa)	(MPa)	(-)	(-)	(s)	(-)
41.2	0.15	3.9	9.7	0.36	81.3	97.6	0.14	2×10^4	5×10^{-6}	292

Figure 1 presents the theoretical (fitted) flow stress surface σ in terms of accumulated viscoplastic strain and strain-rate for both models presented above. In dos Santos model a significant increase in flow stress is observed in strain rates higher than 10^3 s^{-1}. On the other hand, this phenomenon is not taken into account in case of Johnson-Cook model.

NUMERICAL RESULTS

The numerical analysis was carried out using the finite element package ABAQUS/Explicit. An user subroutine VUMAT was used to the implementation of the dos Santos constitutive model.

In this section, two EMF processes were investigated: the high-speed inward tube forming and the high-speed bulging sheet metal. An user subroutine VDLOAD was implemented to model the transient electromagnetic pressure profiles used as loading. An extensive review about the state of the art for these EMF process can be found in Psyk et al. (2011) and Gayakwad et al. (2014).

High-speed inward tube forming

In this section, the high-speed inward tube compression process has been investigated. The geometric model used for this purpose consists of an axisymmetric representation as illustrated in Fig. 2. The tube has initial outer radius $r_o = 7$

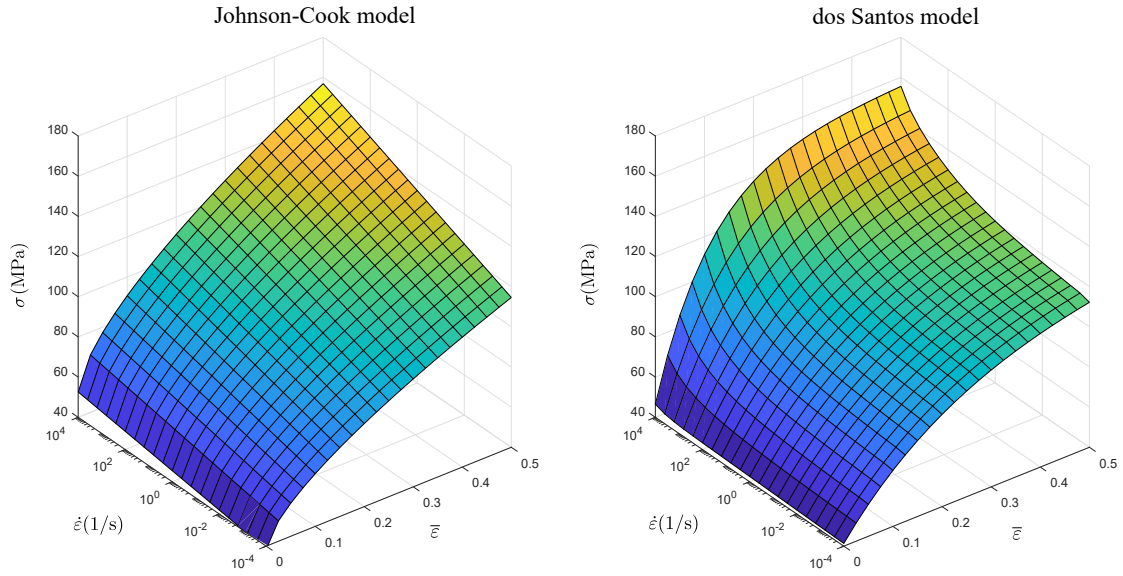

Figure 1 – Flow Stress surfaces in terms of accumulated viscoplastic strain and strain-rate for Johnson-Cook model and dos Santos model for the material parameters defined previously.

mm, inner radius $r_i = 5$ mm, length $l_0 = 25$ mm and load application surface length $w = 8$ mm. Due to symmetric reasons, only one-quarter of tube model was considered, through appropriate boundary condition application. The electromagnetic pressure load was applied in the central portion of the workpiece, toward the minus x-axis, as shown in Fig. 2. The workpiece was discretized using a quadrilateral linear explicit axisymmetric stress element (CAX4R), with reduced integration, where the element controls (e.g. locking, etc.) were set as defaults. The discretization used was of 8 elements trough the thickness and 98 elements along the axis direction. A detail of the employed mesh is illustrated in Fig. 2.

For axisymmetric EMF such as tube compression, a field shaper may also be used with the objective of concentrating and intensifying the magnetic pressure over a localized region of the tube. The resulting pressure pulse p, which magnitude varies on time, but not on the space, can be estimated from the following expression

$$p(t) = \frac{1}{2}\mu \left[\frac{l_a}{n} I(t)\right]^2 c_p \, . \tag{13}$$

given in terms of the magnetic permeability μ, current of discharge I, the fielder shaper concentrator factor cp, the tool coil length l_a and windings number n (see more details in Geier et al. (2014)).

Figure 3 compares mechanical features in the deformed configuration predicted using each of the constitutive models employed. Specifically, Fig. 3(a) presents the comparison regarding the deformed shape at final stage. The simulation employing Johnson-Cook model predicted a outer radius of 4.88 mm, a wall thickness t=2.79 mm and a total length equal to 25.25 mm in the final configuration. In contrast, in the simulation using dos Santos model, outer radius was equal to 5.14 mm, wall thickness t=2.58 mm, and a final length of 25.15 mm were obtained. Figure 3(b) presents the wall thickness variation ratio along the longitudinal direction normalized by the initial length of the tube. It is evident that the thickness increased in the forming region for both models analyzed. A reduction in wall thickness was observed around the normalized length 0.4 for both constitutive models. Clearly, the problem that employed Johnson-Cook model presents the largest variation of thickness along the total length in the almost whole body.

Although both models were calibrated considering the same material data, the corresponding predicted results are distinct. Differences are observed not only regarding displacements, but also, as it would be expected, in terms of stresses and strains. Figure 4 shows the contours plot of von Mises stress and accumulated viscoplastic strain for different time instants during the EMF process for both constitutive models. It can be observed that, during and at the end (after stress stabilization) of the EMF process, the stress and strain fields predicted by each constitutive model were very different. In summary, the Jonhson-Cook model predicted higher von Mises stress and accumulated viscoplastic strain values than dos Santos model.

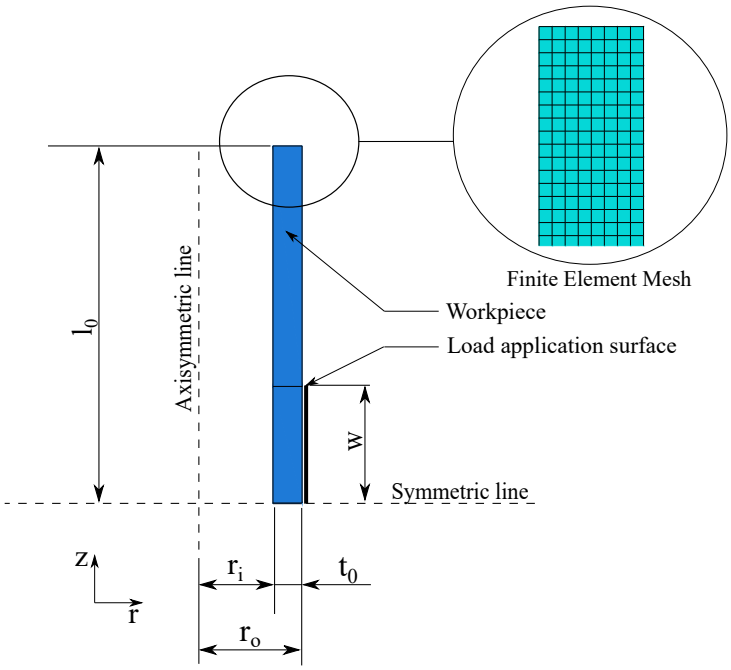

Figure 2 – High-speed inward tube forming: geometry model, finite element mesh and boundary conditions of the electromagnetic inward tube forming process for simulation in ABAQUS/Explicit.

-

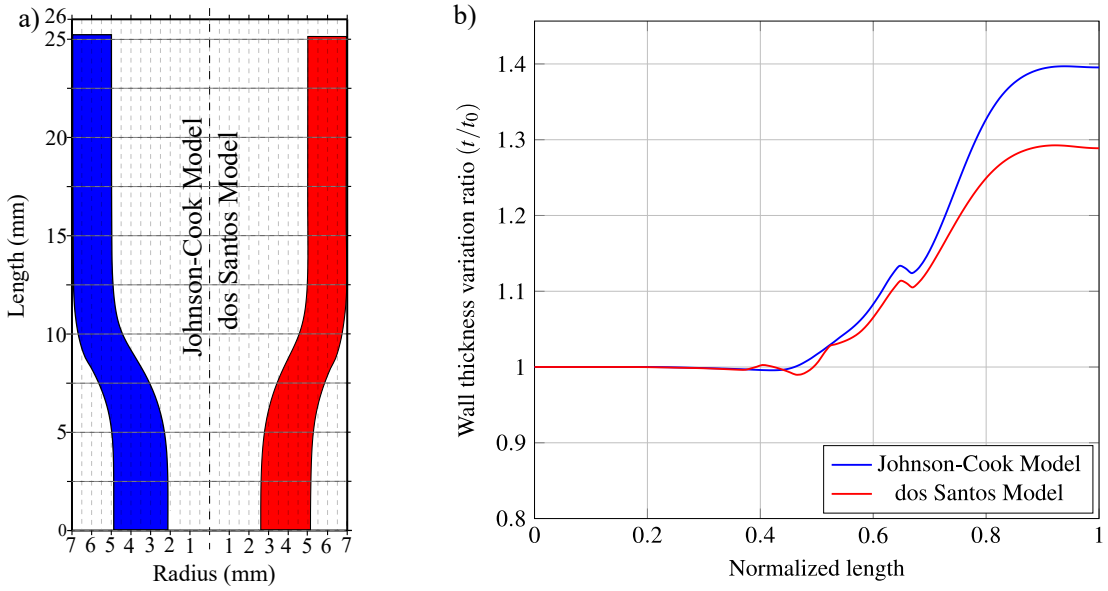

Figure 3 – High-speed inward tube forming: final geometric configuration from both models: (a) Deformed geometry and (b) thickness variation ratio along the tube length.

In order to investigate the stress state distribution at the end of the EMF process, and after stress stabilization, the stresses in radial, tangential and axial directions were plotted at the integration points through the tube wall. Figure 5, shows the stress distribution in the center of the forming region in relation of a radial distance, r, from outward inner tube surface. As it can be seen, the achieved stress states for each constitutive model presented substantial differences.

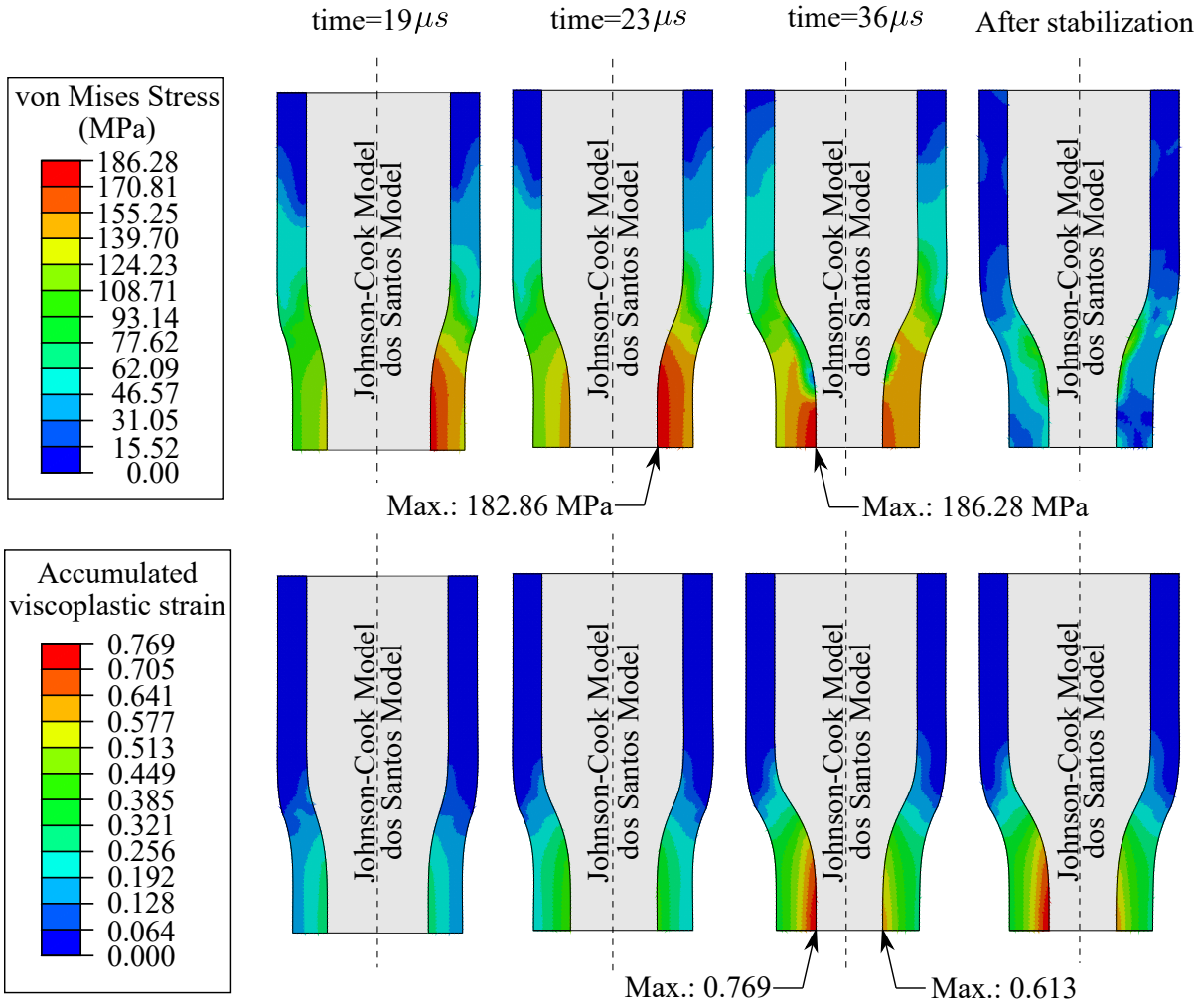

Figure 4 – High-speed inward tube forming: von Mises stress and accumulated viscoplastic strain at various stages of EMF process for the axisymmetric model.

High-speed free bulging sheet metal

In this section, the free bulging sheet metal EMF process was examined. The geometric model consists of an axisymmetric representation as illustrated in Fig. 6. The workpiece was an initial radius r_o = 55 mm and thickness t_0 = 1 mm. The die and the holder were modeled as analytic rigid shells, and the electromagnetic pressure was set on the upper line of the workpiece toward the minus z-axis. A holder force of 12.5 kN was applied to the upper rigid part of the tool, to simulate the compression performed by the preloading phase and a friction coefficient of 0.2 was employed in the simulation, please see Paese et al. (2019) for more details.

The discretization performed here used the same finite element as in the previous EMF case, but now using 4 elements through the thickness and 220 along the radius direction. The values of the electromagnetic pressure distribution were supplied by the in-house software every 0.1 μs, see Paese et al. (2019) for a more detailed explanation. They were interpolated radially, but kept constant during each interval of time. To avoid the need for concordance between the meshes of the electromagnetic problem to the mechanical problem, the electromagnetic pressure was described by a fitting using a sum of sines given by

$$p(r) = \sum_{i=1}^{8} a_i \sin(b_i r + c_i) \tag{14}$$

in which the coefficients a_i, b_i, and c_i were determined using the *cftool* in Matlab® and were kept constant during the

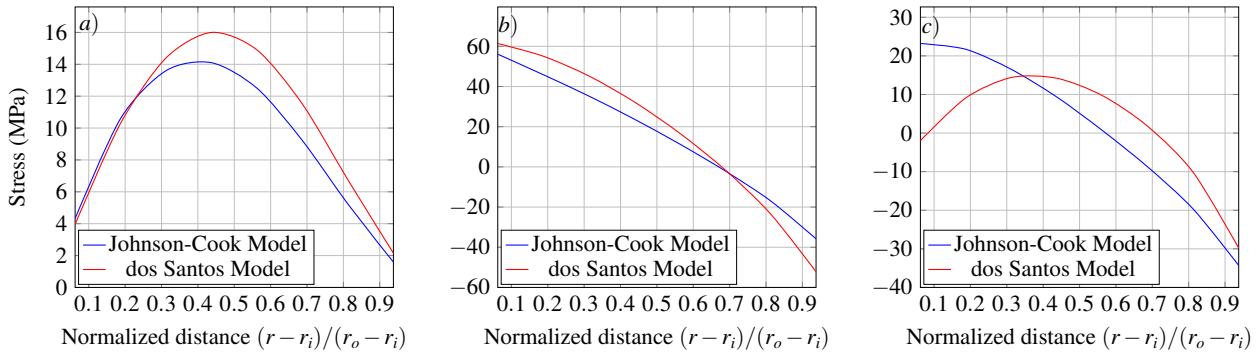

Figure 5 – High-speed inward tube forming; stress after stabilization along the transverse section of thickness in center of the formed workpiece; (a) radial direction, (b) tangential direction and (c) axial direction.

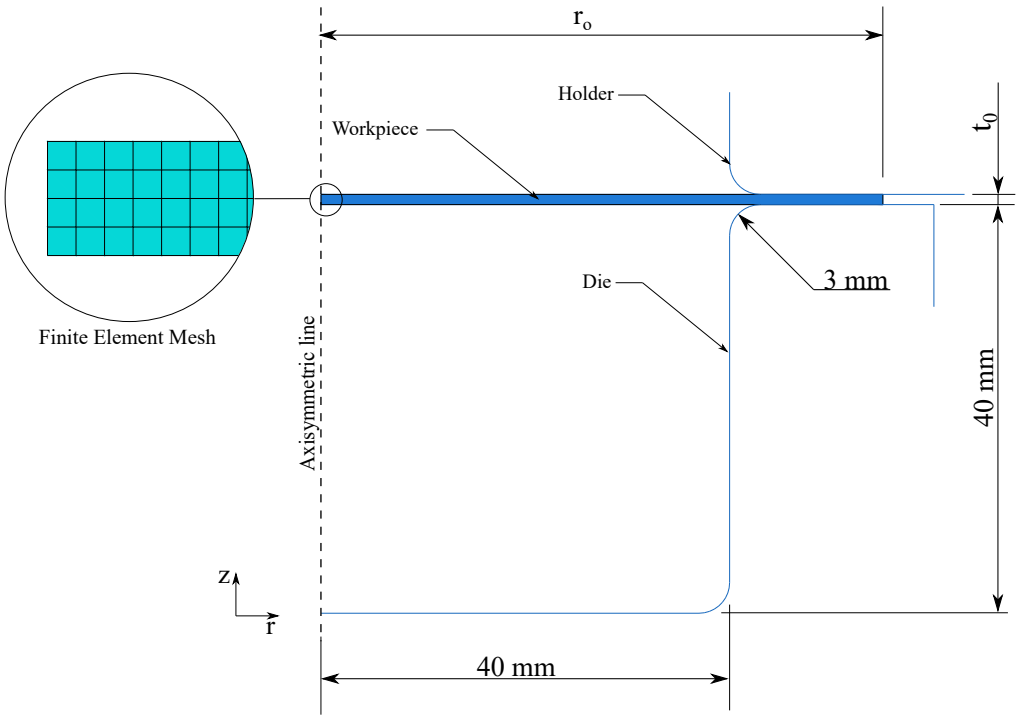

Figure 6 – High-speed free bulging sheet metal: geometry model, finite element mesh and boundary conditions of the EMF free bulging sheet process for simulation in ABAQUS/Explicit.

time increment. Figure 7 shows an example of the fitting used for the electromagnetic pressure profile, using Eq. (14). The electromagnetic pressure was calculated for the energy $U = 1500J$.

Similarly to the previous EMF case, different results were obtained for each constitutive model. Figure 8 shows the contour plots of von Mises stress and the accumulated viscoplastic strain in deformed configuration, for different stages of the bulging EMF process. The analysis that employed the Johnson-Cook model presented a total vertical displacement in the center of the workpiece of 36.52 mm, while for dos Santos model the total displacement was of 35.58 mm. The final thickness in the center of deformed workpiece was t = 0.598 mm for Johnson-Cook model and t = 0.632 mm for dos Santos model.

Figure 9 shows the thickness variation ratio in along the radial coordinate r, having the origin the center of workpiece. The thinnest region occurs in the center of deformed workpiece for both models. The thickness variation along the workpiece length predicted by Johnson-Cook model, as occurred in the previous EMF case, was bigger than for dos Santos model.

Again, stress state distribution after the stress stabilization were investigated. Graphs of the stress state in the center

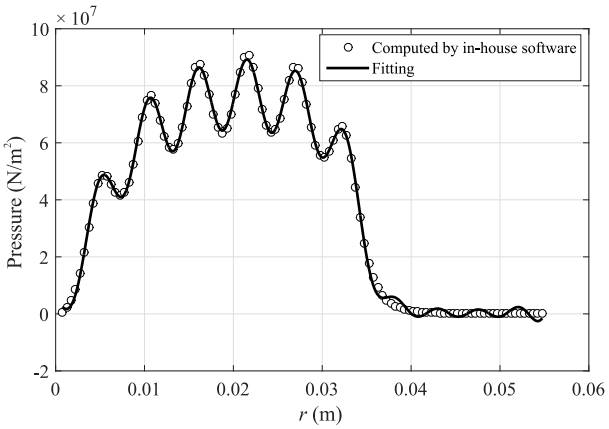

Figure 7 – Electromagnetic profile for the maximum value of the discharge current at time 6.5μs $(U = 1500\text{J})$. The circles are the values of the computed electromagnetic pressure by the in-house software, and the solid line is the continuous fitting, found using Eq. 14 .

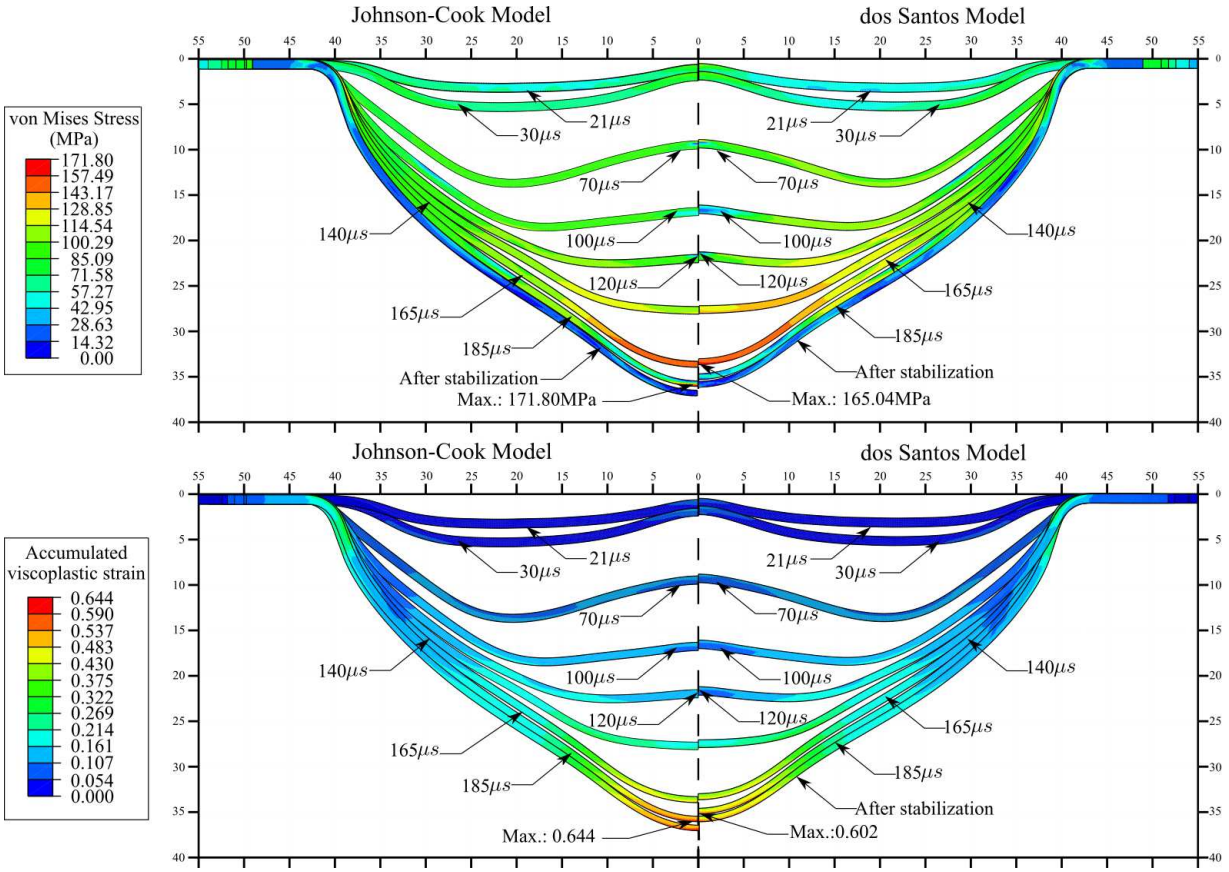

Figure 8 – High-speed free bulging sheet metal: von Mises stress and accumulated viscoplastic strain at various stages of EMF process for the axisymmetric model.

of deformed workpiece in relation the normalized distance across the final thickness are presented in Fig. 10. As before, the stresses after stabilization are very different for each constitutive model used.

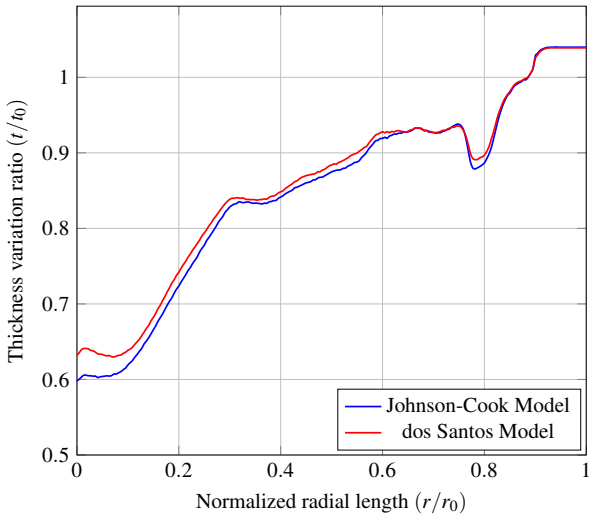

Figure 9 – High-speed free bulging sheet metal: thickness variation ratio in relation the normalized radial distance.

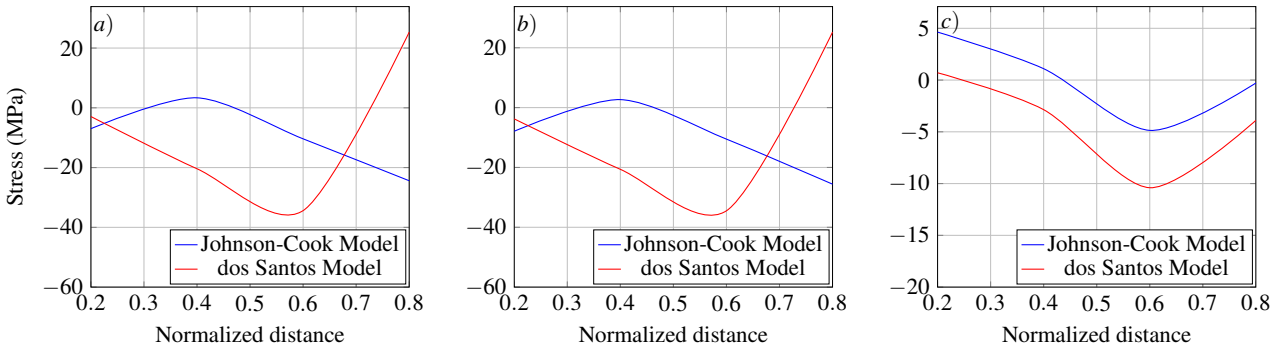

Figure 10 – High-speed free bulging sheet metal: stress after stabilization from upper surface along the transverse section of thickness in the center of the deformed workpiece; (a) radial direction, (b) tangential direction and (c) axial direction.

CONCLUSION

This work has presented an investigation regarding the choice of the constitutive model to be used in high-speed forming simulations. For this purpose, two distinct viscoplastic formulations were adopted, namely Johnson-Cook and dos Santos models. Investigations were conducted considering specific mechanical features, as displacements, stresses, and viscoplastic strains. According to what is reported in the literature, strain-rates in the order of $10^4\ s^{-1}$ can be reached in high-speed forming processes. For such high-velocity processes, strain-rate hardening effects are expected to play an important role. Therefore, given the fact that the hardening behavior has a direct influence on both the stress response and inelastic evolutions, major differences between the two approaches were evidenced for the cases considered in this work.

Although both constitutive models were calibrated for the same material experimental data the achieved final states in terms of the workpiece movement, strains, stresses, and internal variables are quite different depending on the choice of the constitutive model once the Johnson-Cook model does not account for the strain-rate hardening.

Such points can be evidenced along the results depicted in this work but, for instance, comparing the final stresses in the components, Figs. 5 and 10, one can clearly note that the stress distributions are quite different. The same is true for the accumulated plastic strain. This implies that the predicted material state is different regarding the choice of the constitutive model. Therefore, pronounced influences are also expected on the predicted forming limit or estimated fatigue life of dynamically deformed components.

Finally, based on the results previously reported, in an effort to provide a better understanding the mechanical behavior, it is clear that further investigations have to be conducted. Future works should consider the experimental characterization of the hardening response throughout the workpiece. In addition, predictions using other constitutive models should also

be obtained and compared to the present results.

ACKNOWLEDGMENTS

The author Andrey Brezolin wishes to acknowledge the master scholarship supported by CAPES, Coordenação de Aperfeiçoamento de Pessoal de Nível Superior. The author Rodrigo Rossi wishes to acknowledge the support of *CNPq*, Conselho Nacional de Desenvolvimento Científico e Tecnológico of Brazil (Grant number 304044/2015-6).

REFERENCES

Follansbee, P., & Kocks, U., 1988, "A constitutive description of the deformation of copper based on the use of the mechanical threshold stress as an internal state variable". Acta Metallurgica, Vol. 36, pp. 81 – 93.

Gayakwad, D., Dargar, M. K., Sharma, P. K., purohit, R., & R.S.Rana, 2014, "A review on electromagnetic forming process". Procedia Materials Science, Vol. 6, pp. 520 – 527.

Geier, M., José, M. M., Rossi, R., Rosa, P. A. R., & Martins, P. A. F., 2014, "Interference-fit joining of aluminium tubes by electromagnetic forming". Advanced Materials Research, Vol. 853, pp. 448 – 493.

Johnson, G., & Cook, W., 1983,. "A Constitutive Model and Data for Metals Subjected to Large Strains, High Strain Rates, and High Temperatures". In *Proceedings 7th International Symposium on Ballistics* (pp. 541–547). The Hague.

Molinari, A., & Ravichandran, G., 2005, "Constitutive modeling of high-strain-rate deformation in metals based on the evolution of an effective microstructural length". Mechanics of Materials, Vol. 37, pp. 737 – 752.

Paese, E., Geier, M., Homrich, R. P., Rosa, P., & Rossi, R., 2019, "Sheet metal electromagnetic forming using a flat spiral coil: Experiments, modeling, and validation". Journal of Materials Processing Technology, Vol. 263, pp. 408 – 422.

Perić, D., 1993, "On a class of constitutive equations in viscoplasticity: Formulation and computational issues". International Journal for Numerical Methods in Engineering, Vol. 36, pp. 1365–1393.

Perzyna, P., 1966,. "Fundamental problems in viscoplasticity". (pp. 243–377). Elsevier volume 9 of *Advances in Applied Mechanics*.

Perzyna, P., 1971,. "Thermodynamic theory of viscoplasticity". (pp. 313–354). Elsevier volume 11 of *Advances in Applied Mechanics*.

Psyk, V., Risch, D., Kinsey, B., Tekkaya, A., & Kleiner, M., 2011, "Electromagnetic forming—a review". Journal of Materials Processing Technology, Vol. 211, pp. 787 – 829.

dos Santos, T., 2016,. *Experimental characterization and constitutive modeling of a viscoplastic effects in high strain-rate deformation of polycrystalline FCC metals*. Ph.D. thesis Universidade Federal do Rio Grande do Sul.

dos Santos, T., Rosa, P. A., Maghous, S., & Rossi, R., 2016, "A simplified approach to high strain rate effects in cold deformation of polycrystalline fcc metals: Constitutive formulation and model calibration". International Journal of Plasticity, Vol. 82, pp. 76 – 96.

RESPONSIBILITY NOTICE

The authors are the only responsible for the printed material included in this paper.